Journal of Materials Chemistry A

Accepted Manuscript

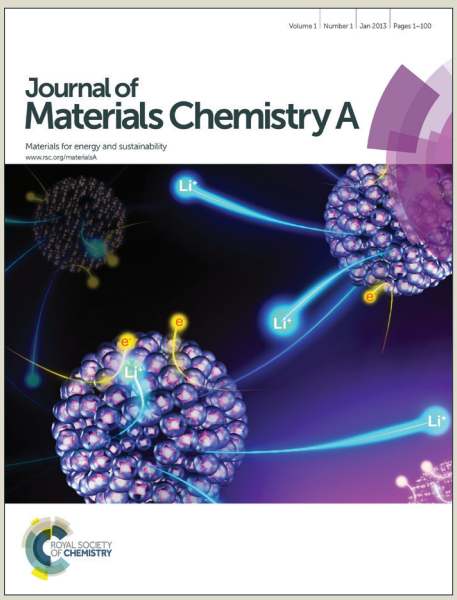

ROYAL SOCIETY OF CHEMISTRY

www.rsc.org/materialsA

Electrochemical synthesis of highly corrugated graphene sheets for high performance supercapacitors

Amr M. Abdelkader

School of Materials and School of Chemistry, University of Manchester, Oxford Road, M13 9PL, UK

Abstract:

Highly corrugated graphene sheets with low susceptibility to re-stacking were prepared by electrochemical reduction of graphene oxide (GO) in a molten salt bath. Oxygen functional groups were removed by depositing the reducing agent on a GO assembled cathode and also by direct electro-deoxygenation without generating reducing agents. The produced graphene derivative had electrical conductivity as high as 2300 S/m, and a specific surface area of 565 m^2/g making it ideal as a supercapacitor with maximum specific capacitance of 255 F/g in 6 M KOH aqueous solution without the need for doping the graphene sheets. Further, the supercapacitor showed excellent cycling stability, retaining 95% of its initial capacitance after 5000 cycles of charge/discharge. Therefore, this material presents great promise for future design and large-scale production of affordable and high performance graphene electrodes for portable energy storage devices.

Introduction

Since its initial fabrication by micro-mechanical cleavage, graphene, a single-atom-thick sheet of hexagonally arrayed sp^2-bonded carbon atoms, has attracted tremendous interest and shown great promise for many potential applications, particularly for energy harvesting and storage.[1, 2] Graphene is considered to be a strong candidate for fabricating high-performance electrochemical double-layer (EDLC) supercapacitors because of its excellent electrical conductivity and high theoretical specific surface area (~2600 m^2/g).[2-5] Depending on the fabrication of the electrodes, a great part of this theoretical surface area can be made accessible to the electrolyte, which significantly increases the capacitance. Recently, a great deal of effort has been devoted to exploring graphene-based supercapacitors. Free-standing graphene foam grown by chemical vapour deposition has shown high rate capability.[6] Reduced graphene oxide (GO) represents a cheap alternative that can be produced in large quantities. Many methods have been used to reduce GO and fabricate EDLC) supercapacitor electrodes. For example, reduction of graphene hydrogels with hydrazine or hydroiodic acid produced materials that gave high specific capacitance of 220 F/g, but the materials lost 30% of their capacitance in the first few hundred cycles.[7,8] Thermal reduction of GO at 1050°C under argon was used to fabricate EDLC with specific capacitance of 177 F/g.[9] Reduction with microwave irradiation produced electrodes with reasonably good cyclability, and specific capacitance ranged between 200 and 210 F/g.[10] Solvothermal reduction in Dimethylformamide at 150°C produced graphene with high oxygen content that enhanced the specific capacity to 276 F/g in aqueous solution.[11] Similarly, GO paper reduced with urea at 95°C showed specific capacitance as high as 255 F/g due to the presence of residual oxygen groups.[8] However, these kinds of pseudocapacitance-enhanced electrodes suffer from low cyclability.

Graphene in general, and graphene produced via the reduction of GO in particular, tends to form irreversible agglomerates through van der Waals interaction, resulting in inaccessible surfaces and loss of capacitance in comparison with the expected theoretical values (550 F/g).[12, 13] Several strategies have been examined to minimise the aggregation of the graphene sheets. Functionalising graphene with conductive

polymers, metal or metal oxides/hydroxide prevented re-stacking of the graphene sheet.[14-20] However, the electrochemical stability of the supercapacitor often becomes poor due to the inherent instability of doped species under the electrochemical conditions. Using curved and corrugated graphene is a promising solution to prevent aggregation.[4] Reducing graphene oxides with reactive metals in molten salts has shown great ability to heal defects introduced through the oxidation process and to restore the unique properties of graphene.

This study presents a novel, rapid and affordable technique to produce crumbled graphene sheets via electrochemical reduction of GO at moderate temperature. The study also shows that oxygen functional groups could be effectively removed without the need to generate a reducing agent via a direct electro-deoxidation and dehydration mechanism. The unique morphology of the produced graphene showed a specific surface area of approximately 565 m^2/g and specific capacitance of 255 F/g.

Results and discussion

The ability of alkali metals to remove oxygen functional groups from the GO surface has been proven in previous work. [21] The presence of molten salts that are able to dissolve the oxygen-containing by-products of the reduction process significantly facilitated the reduction.[21] Since most alkali metals are commercially produced via molten salt electrolysis of their halides, it was logical to generate the reducing agent in situ during the reduction. The LiCl–KCL system has a melting point of 350°C at the eutectic composition,[22] which allows the generation of elemental Li and/or K at the cathode at low temperature according to equation (1).

$$Li^+ + e^- = Li \qquad (1)$$

The by-products of the GO reduction reactions ($LiCO_3$, LiOH, Li_2O) should also be soluble in the eutectic mixture. To prove this concept, a potential of 3.5 V was applied between the stainless steel cup cathode holding a porous GO pellet and a Pt wire anode for 1 hour. The powder collected after the process was then subjected to X-ray photoelectron spectroscopy (XPS) analysis to investigate the efficiency of the electro-reduction process. Figure 1 shows the C1s spectra of GO and electro-reduced

graphene oxide (LiER-GO) samples. The C1 spectrum of the original GO (Figure 1a) revealed that it consisted of two main components arising from C–O groups (hydroxyl and epoxy, ~286.5 eV) and the C–C bond (~284.6 eV), and two minor components from C=O (carbonyl, ~288.3 eV) groups and O–C=O (carboxyl, ~290.3 eV) groups.[23, 24] After the electro-reduction, the LiER-GO exhibits a similar XPS spectrum to natural graphite (Figure S3 in the supporting Information); C=C bonds dominate, as shown by a single peak with small tails at the higher-binding energy region,[23] confirming good restoration of C=C bonds in the LiER-GO. The small bump around 288.5 eV in the LiER-GO curve indicated some residual oxygen functionality and it was within the ketone and carboxyl carbon region.

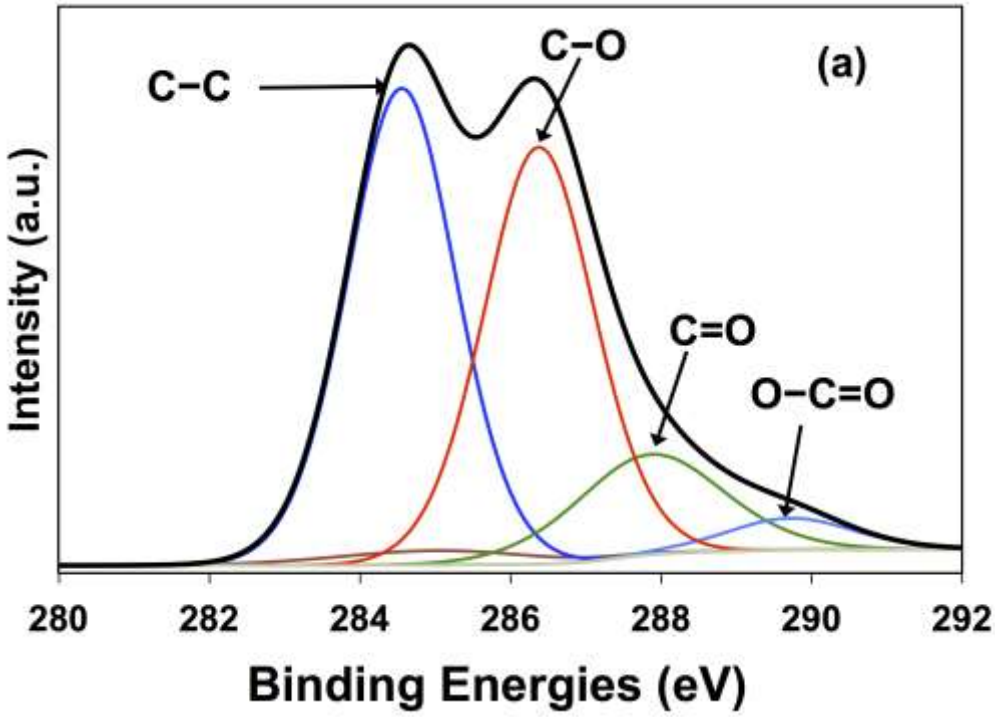

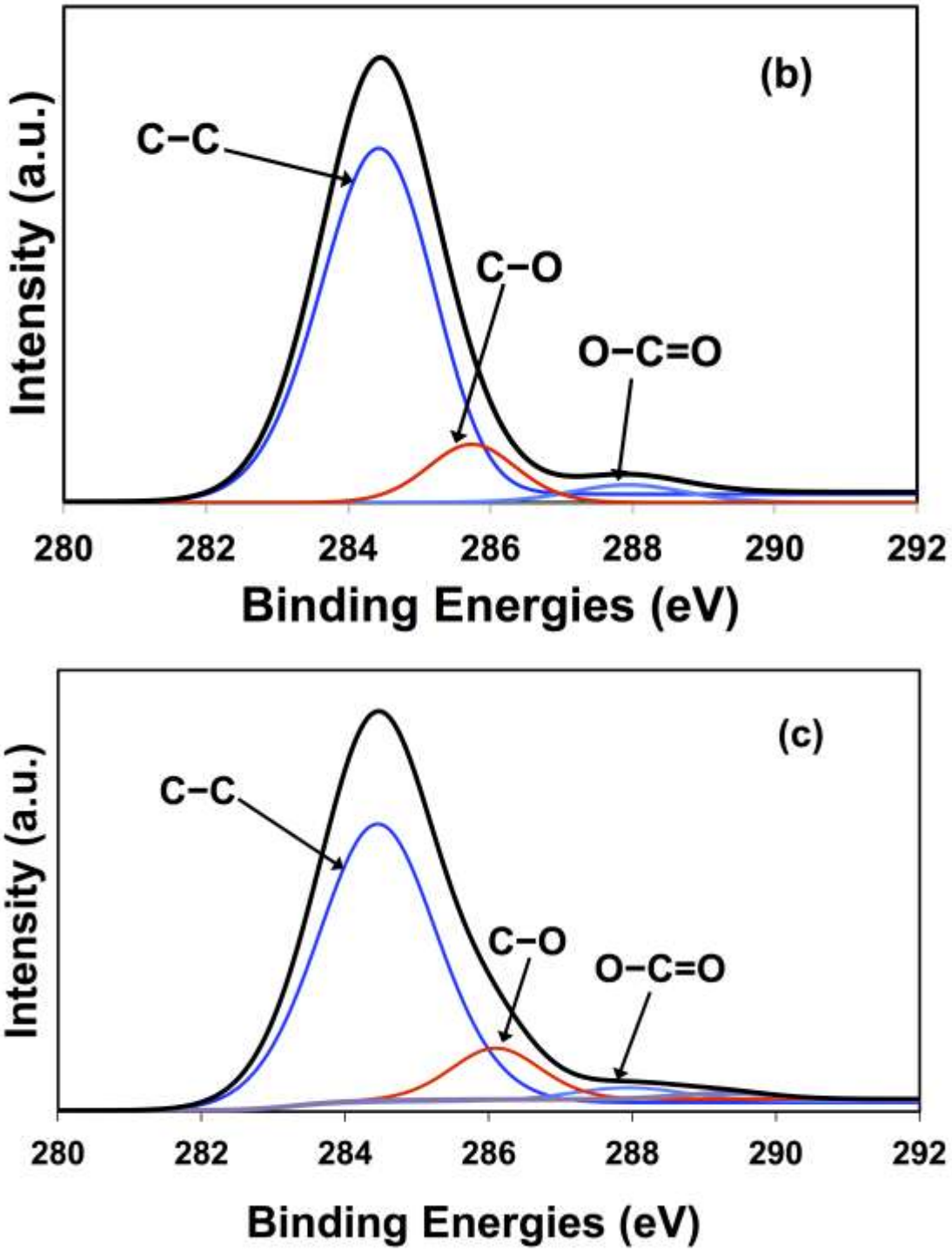

Figure 1: XPS C1 peak comparison of (a) GO, (b) LiER-GO, and (c) EDoX-GO. The corresponding deconvoluted peaks are also shown for each case.

From a thermodynamic point of view, the reduction of most solid oxides takes place at cathodic potential lower than that required to generate alkali metals.[25] Reducing GO without the need to generate the reducing alkali metal has economic, engineering and environmental advantages. Generating alkali metals increases the

electronic conductivity of the molten salt and consequently increases the non-faradaic current and parasitic reactions raising energy consumption. In addition, conducting the reduction at lower potential eliminates the risk of generating Cl_2 gas (or other halogen gases) at the anode. To test this concept, a constant voltage of 2 V was applied between the GO cathode and Pt anode for 1 hour. This voltage is lower than that reported to dissociate LiCl or KCl.[26, 27] The duration of the electrolysis time was selected based on the recorded response of the electrode over time (Figure S4 in the supporting Information). The electrochemically deoxygenated GO (EDoX-GO) was subjected to a number of physical characterisation methods to evaluate the efficiency of the process.

XPS analysis provided clear evidence of the reduction. The high resolution C1 peak (Figure 1c) revealed that the majority of the oxygen-containing groups in GO were removed and the C–C bond becomes dominant, as shown by the single peak with a small tail in the higher-binding energy region. The C/O ratio was 12.5, which is higher than that reported for GO reduced by many other methods (see Table S1 in the Supporting Information) and comparable to the GO reduced by electrochemically generated Li, strongly suggesting that the removal of oxygen-containing groups can be achieved via direct electro-deoxidation without the need for any reducing agent.

The colour of the powder changed from yellow-brown to black after electrochemical deoxygenation. The dispersion of the reduced powder in pure water was not stable, indicating the removal of the hydrophilic functional groups. However, unlike GO reduced by other chemical methods,[28] the EDoX-GO was dispersible into solutions of surfactants, such as sodium dodecylsulfate (SDS), sodium dodecylbenzenesulfonate (SDBS), centrimonium bromide (CTAB), and TRITON X-100, after mild sonication for only 5 min. The EDoX-GO suspensions were stable for a month without visible precipitation (Figure 2), indicating that the EDoX-GO did not undergo irreversible aggregation.[29, 30] A concentration of 1 mg/ml was obtained in SDBS solution, which is greater than that obtained by re-dispersing the hydrazine-reduced GO.

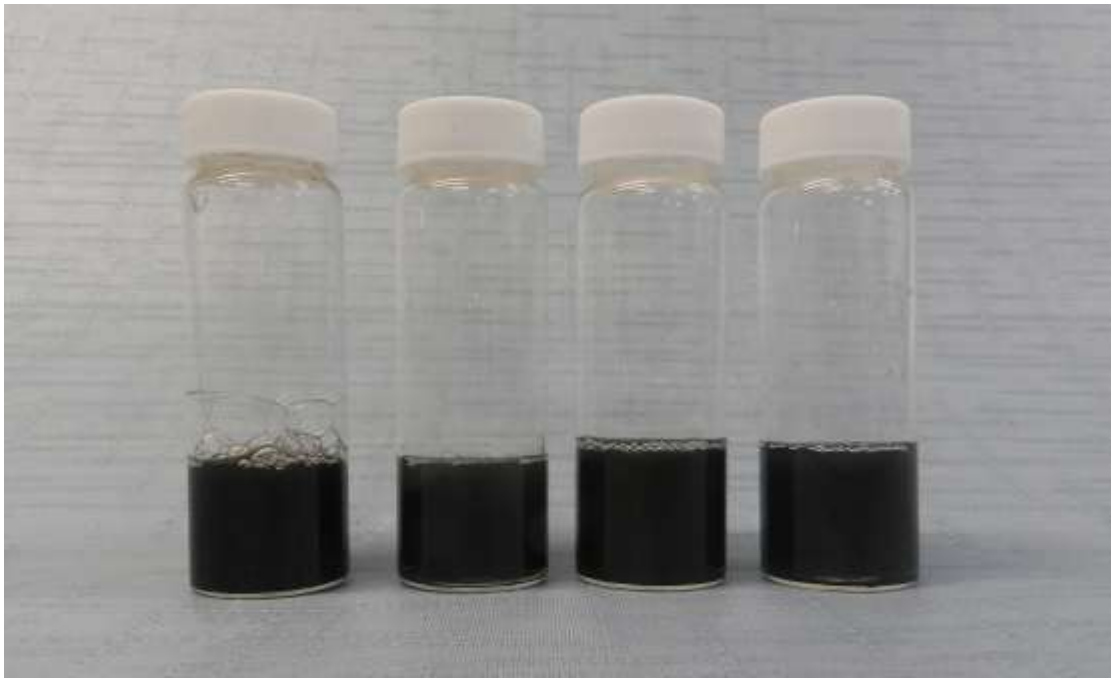

Figure 2: Digital images of EDoX-GO dispersed on aqueous solutions of SDS, SBDC, CATB, and TRITON X-100 (from left to right)

Thermogravimetric analysis (TGA) provides further proof of the electrochemical deoxygenation and dehydration of GO. Figure 3 reveals the TGA curves under nitrogen flow with a heating rate of 1°C/min for GO, and the produced powder after 1 hour of electrolysis at 2 V. The TGA curve for the original GO exhibited two peaks for mass loss with increasing temperature. The first peak at around 100°C showed a mass loss of about 9% and can be attributed to the removal of adsorbed water from the GO surface.[31] The mass loss peak of approximately 30% at around 200°C can be attributed to the decomposition of labile oxygen functional groups forming O_2, CO, CO_2 and H_2O gases.[31] The electrochemically deoxygenated powder exhibited much higher thermal stability compared with GO. After electrochemical deoxygenation the weight loss up to 100°C was approximately 1%, indicating that EDoX-GO powder did not contain as much water as previously reported.[32] In addition, the EDoX-GO TGA curve did not have mass loss peaks around 200°C, which indicates that the reduction of GO was nearly complete. The gradual weight loss of about 7% below 500°C is likely due to the loss of residual functional groups on the EDoX-GO.

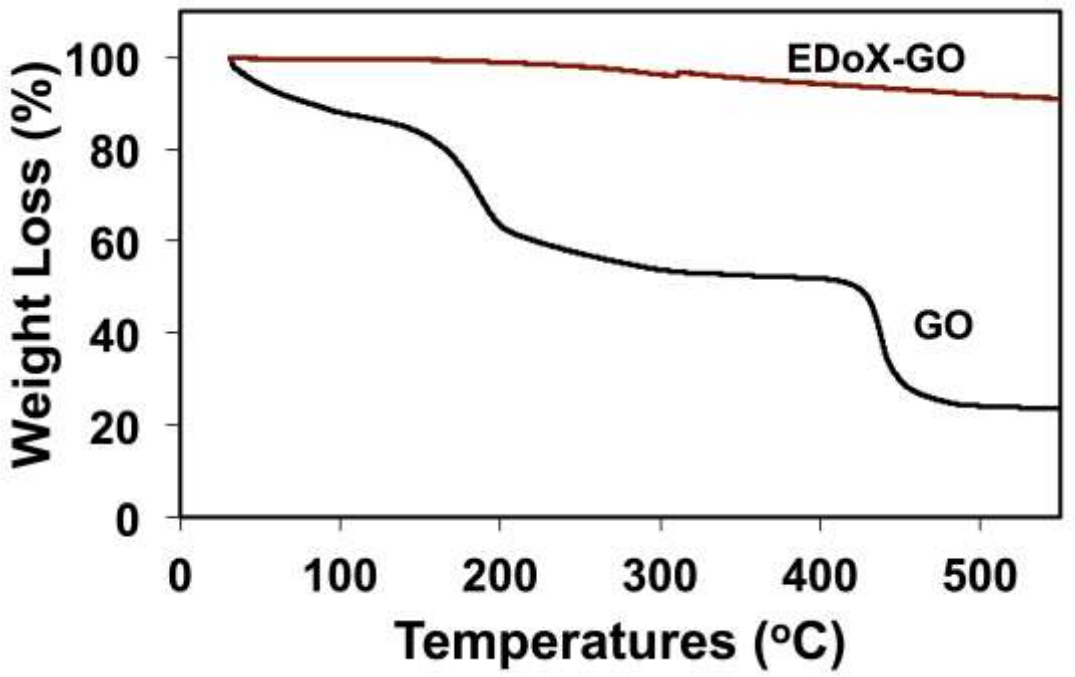

Figure 3: TGA plot of GO and electro-deoxygenated graphene. The sample after the electrochemical treatment showed clear thermal stability.

An important parameter to evaluate the structure of graphene-based materials is the distance between two layers. The X-ray diffraction (XRD) pattern of the as-synthesised GO powder (Figure 4) showed a single peak at ~10° 2θ corresponding to an interlayer *d* spacing of ~0.8 nm. This can be attributed to the expansion of the 0.34 nm spacing between typical graphene sheets in the graphite gallery due to water molecules trapped between oxygen-containing functional groups on GO sheets.[33] After electro-deoxygenation, the peak at 10° 2θ completely disappeared and a hump centred at approximately 25° 2θ was observed, corresponding to an interlayer spacing of about 0.36 nm. The width and the shape of the peak in the XRD pattern of the EDoX-GO can be attributed to the relatively short domain order or turbostratic arrangement of stacked sheets.

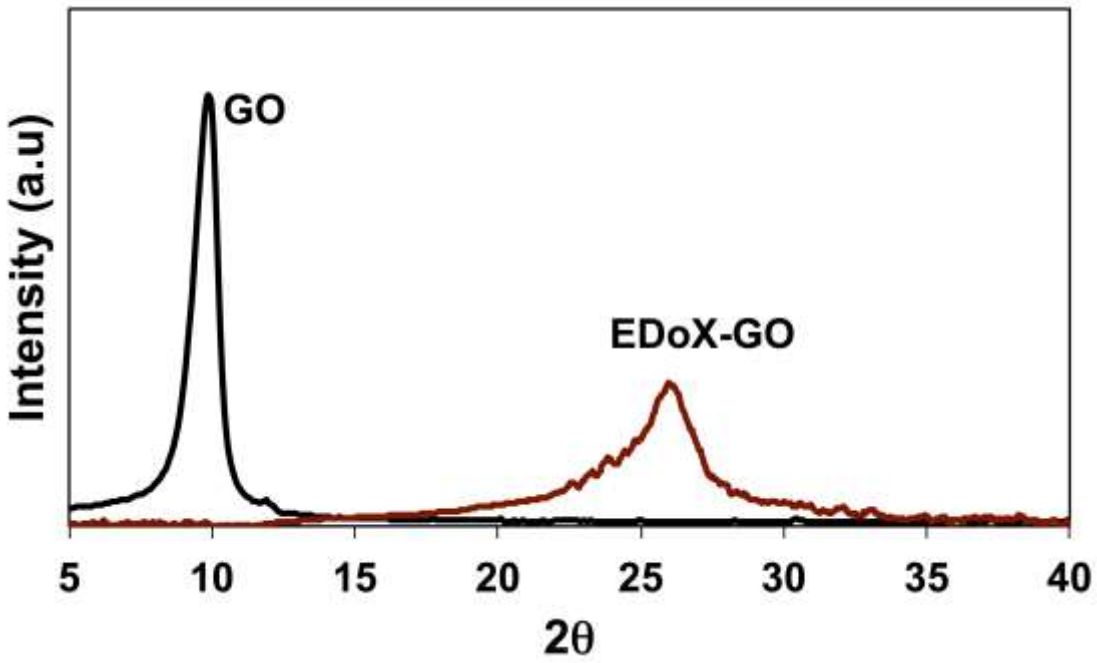

Figure 4: XRD spectra of GO and EDoX-GO highlighting the shift of the (002) diffraction peak due to the reduction process.

FT-IR spectra of the original GO and the EDoX-GO are shown in Figure 5. The characteristic peaks of GO can be observed: (1) C=O stretching vibration at 1746 cm^{-1}; (2) the O–H stretching and deformation vibrations at 3420 cm^{-1} and 1395 cm^{-1} respectively; (3) aromatic C=C stretching vibration at 1625 cm^{-1}; (4) epoxy C–O stretching vibration at 1220 cm^{-1}; and (5) the alkoxy C–O stretching vibration at 1053 cm^{-1}.[34] After electro-deoxygenation the peaks for oxygen functional groups almost vanished, confirming their efficient removal. The peak at 1625 cm^{-1} corresponding to the aromatic C=C group was still present, suggesting that the frame of sp^2-bonded carbon atoms was retained well after electro-deoxygenation.

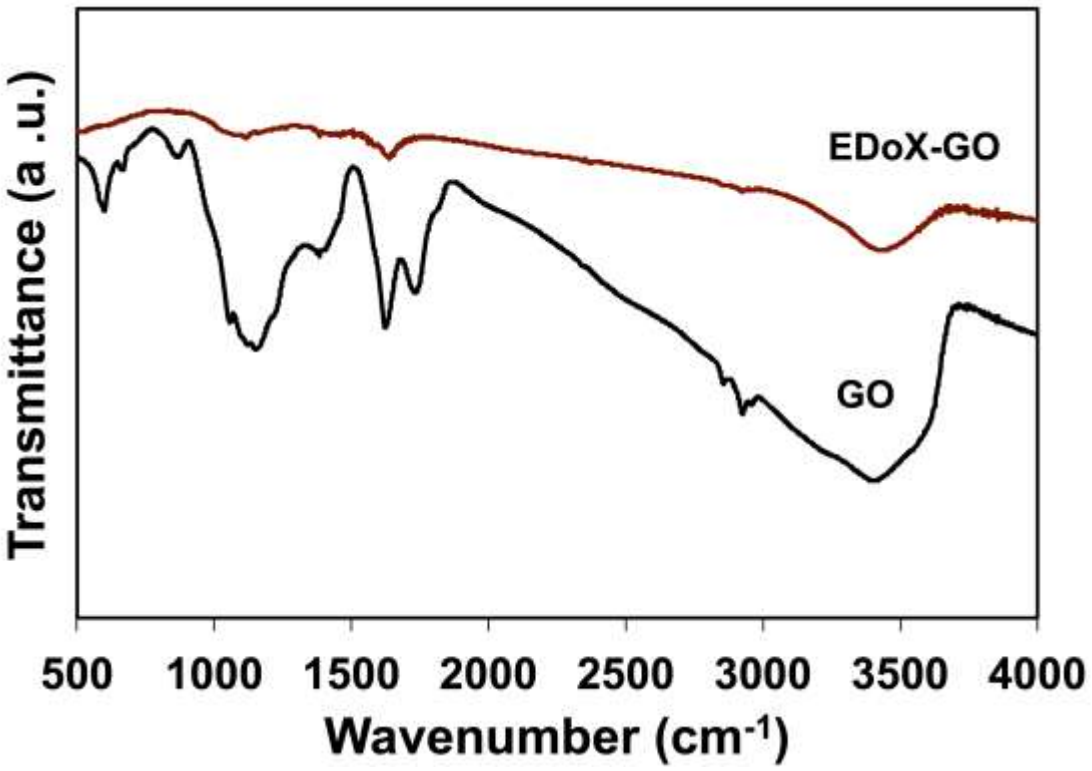

Figure 5: FTIR plots for GO and EDoX-GO showing effective removal of the oxygen functional groups by the direct electro-deoxidation process.

Raman spectroscopy provides a useful tool to characterise graphitisation and the intensity of defects in carbon nanomaterials. In general, pristine defect-free graphite shows two bands: one at 1580 cm^{-1} (the G band) arises from the first order scattering of the E_{2g} phonon of sp^2-bonded carbon atoms; and a band at ~2600 cm^{-1} (the 2D band) corresponding to the double-resonance process.[35, 36] Upon introducing defects, such as those associated with oxidation, the intensity of the 2D band decreases and another band appears at ~1330 cm^{-1} (called the D band), associated with the vibrations of carbon atoms with sp^3 electronic configuration of disordered graphene.[37] Figure 6 shows the Raman spectra of GO and EDoX-GO. The Raman spectrum for the original GO exhibited a broad G band at 1575 cm^{-1} possibly due to the presence of isolated double bonds resonating at higher frequencies than the G band of graphite.[35] In addition, the D band at ~1333 cm^{-1} became prominent, implying a reduction in size of the in-plane sp^2 domains owing to extensive oxidation. After electrochemical de-oxygenation of GO, the sheets did not show any noticeable decrease in the D/G ratio. This observation suggests that the reduction process did not create more lattice defects associated with the removal of the carbon atoms to

form CO, CO_2, or CO_3^{2-} during reduction and predominantly defined intact graphene regions.[38] This means that the removal of the oxygen functional groups may have occurred without formation of carbon-containing products.

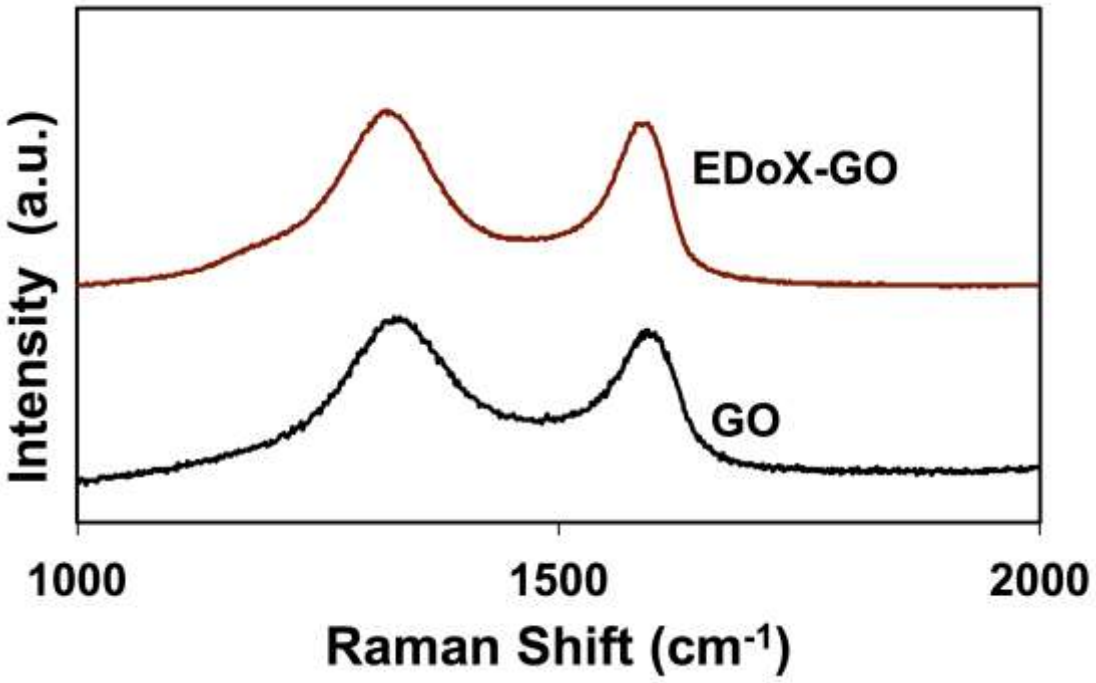

Figure 6: Raman spectra of GO and EDoX-GO showing no increase of the D band intensity indicative of a non-destructive reduction process.

Electrical conductivity of the reduced products is another important criterion to evaluate the quality of reduced GO. Original GO is an insulator, with a conductivity of less than few mS/m. After electrochemical deoxygenation, the conductivity of a film prepared from the EDoX-GO powder via vacuum filtration was about 2300 S/m, clearly indicating efficient restoration of the conducting properties of graphene. Annealing of EDoX-GO paper at 600°C under argon led to a further increase in conductivity to 5230 S/m, two orders of magnitude greater than that of graphite powder. Conductivity was measured using a standardised four-point probe to eliminate contact resistance, and each paper was cut into a rectangular shape and measured three times to obtain an average value.

To fabricate materials with high surface area suitable for supercapacitor electrodes, the sample was quenched to room temperature after electro-deoxygenation by lifting the cathode to the water-cooled top part of the reactor. Scanning electron microscopy (SEM) images (Figure 7) showed fluffy and heavily corrugated graphene sheets with numerous wrinkles and folded regions. These crumpled graphene sheets

were loose and had little tendency to form clusters of disordered solid as reported for other reduction methods,[39] confirming that curved and crumpled graphene sheets can effectively prevent face-to-face re-stacking of the sheets. In addition, the specific surface area of the EDoX-GO sample measured by the BET method was 565 m^2/g, further confirming that the corrugated graphene sheets can effectively minimise van der Waals re-stacking. This morphology and high surface area are favourable for fast diffusion and migration of electrolyte ions into the surfaces of graphene sheets to form electric double layers during fast charge/discharge processes. BJH analysis showed (figure S9 in the supporting information) that the pore sizes of the EDoX-GO sample mainly center around 3.2 nm. It is well known that the uniform pore sizes in the range of 3–5 nm are required to improve the capacitance in EDLCs. [40, 41]

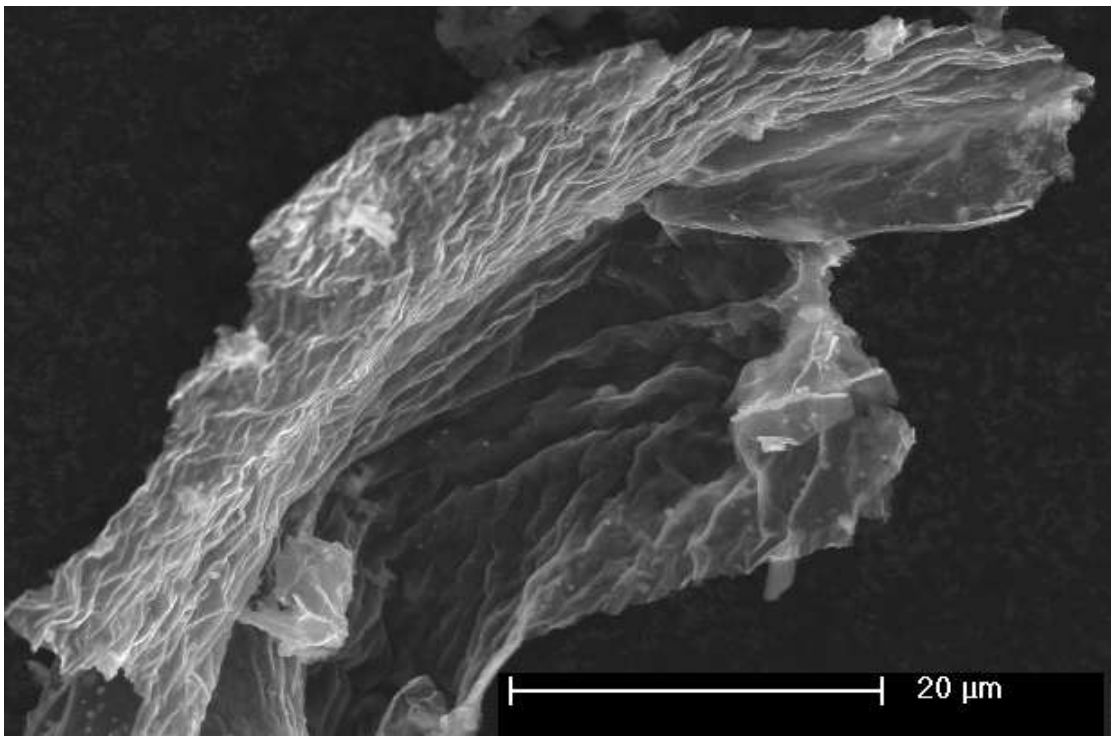

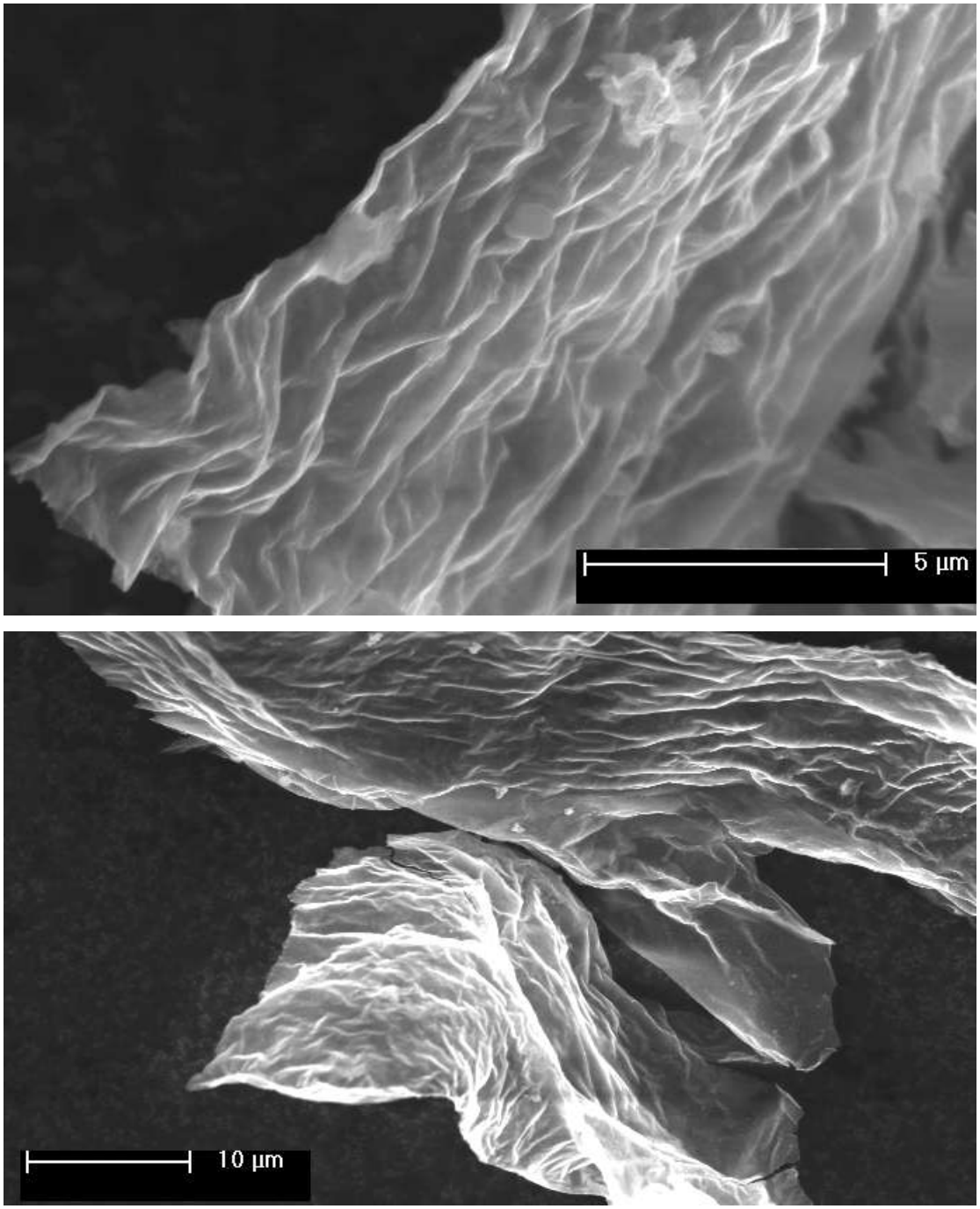

Figure 7: SEM images of the crumpled and heavily wrinkled graphene sheets produced *via* the direct electro-deoxidation approach. The SEM images showed lack of flake-aggregation, as can be seen in (c) where individual flakes can be identified (see the supporting information for more images).

Electrochemical performance

The performance of the supercapacitor electrode was assessed by cyclic voltammetry and galvanostatic charge/discharge tests in a two-electrode configuration. Figure 8a shows the cyclic voltammogram (CV) curves of the EDoX-GO at different scan rates ranging from 20 to 150 mV/s mV/s of a potential range of 0 to

1 V in 6 M KOH solution. All the CV curves exhibited a nearly ideal rectangular shape, indicating that specific capacitance primarily originated from double-layer capacitance based on ions adsorption/desorption. The absence of any obvious redox peaks was an indication of the efficient removal of the oxygen functional groups during electro-deoxygenating, and therefore the contribution of pseudocapacitance was negligible. With increasing scan rate, CV curves presented good mirror images with respect to the zero-current line and a symmetric I–E response at both positive and negative polarisations, implying fast charge transfer within the electro-deoxygenated materials as a result of the highly corrugated graphene sheet morphology. Even at a high scan rate of 150 mV/s the CV curves remained nearly rectangular without obvious distortion.

Galvanostatic charge/discharge curves were also recorded for practical capacitance evaluation in alkali electrolyte. EDoX-GO retained nearly linear and symmetric charge/discharge profiles even at high current density (Figure 8b). These observations are consistent with the results of CV measurements, further indicating the excellent capacitive behaviour of EDLC. Moreover, the EDoX-GO displayed almost no drop in IR at the beginning of the discharge curve, indicating low overall internal resistance of the electrode due to the removal of the oxygen functional group. The corresponding specific capacitance was calculated from the slopes of the discharge branch of the curve. The correlation between the specific capacitance and the various current densities is presented in Figure 8c. The EDoX-GO supercapacitor had a specific capacitance as high as 255 F/g at 0.25 A/g. This value is greater than that calculated for capacitors made of GO reduced by lithium in molten LiCl–KCl (205 F/g),[21] and by the lithium generated electrochemically at the cathode in molten LiCl–KCl (230 F/g, Figure S8 in the supporting Information) at the same reduction temperature and discharge current density. The higher specific surface area of the EDoX-GO explains the enhancement of the specific capacitance.

The cycling durability of EDoX-GO in aqueous electrolyte as determined from the charge/discharge curve is presented in Figure 8d. The EDoX-GO retained ~95% of its initial capacitance in the first 5000 charging/discharging cycles, indicating that the electrode has good electrochemical stability and a high degree of reversibility in the repetitive charge/discharge cycling test. This result was also confirmed by comparing

the shape of the cyclic voltammograms recorded before cycling and after 5000 cycles of charging/discharging (Figure S7 in the supporting Information).

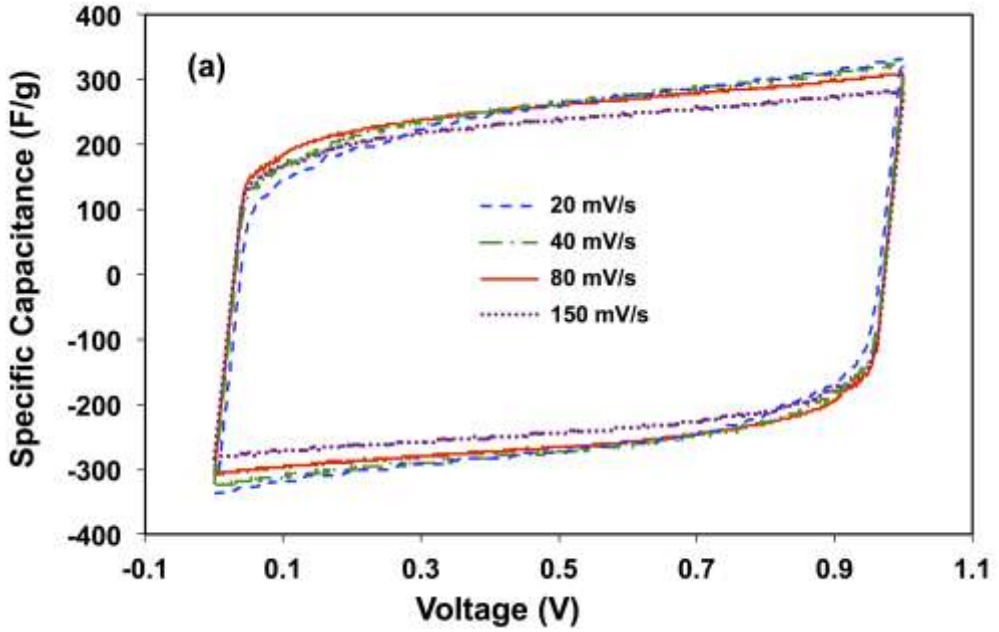

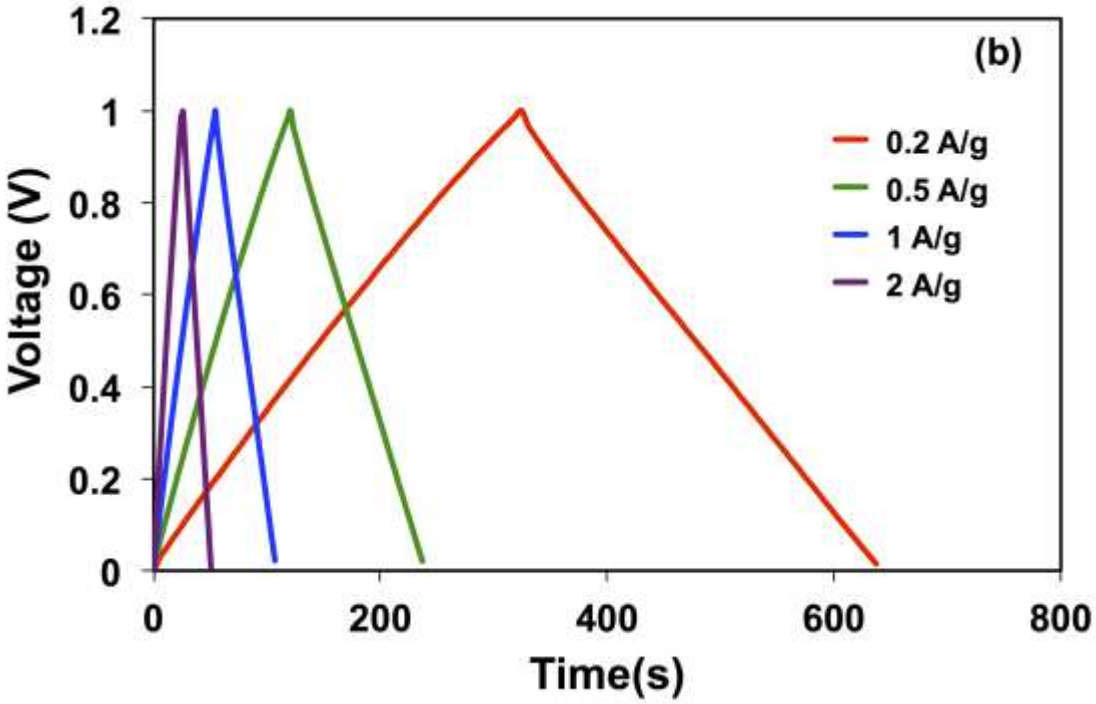

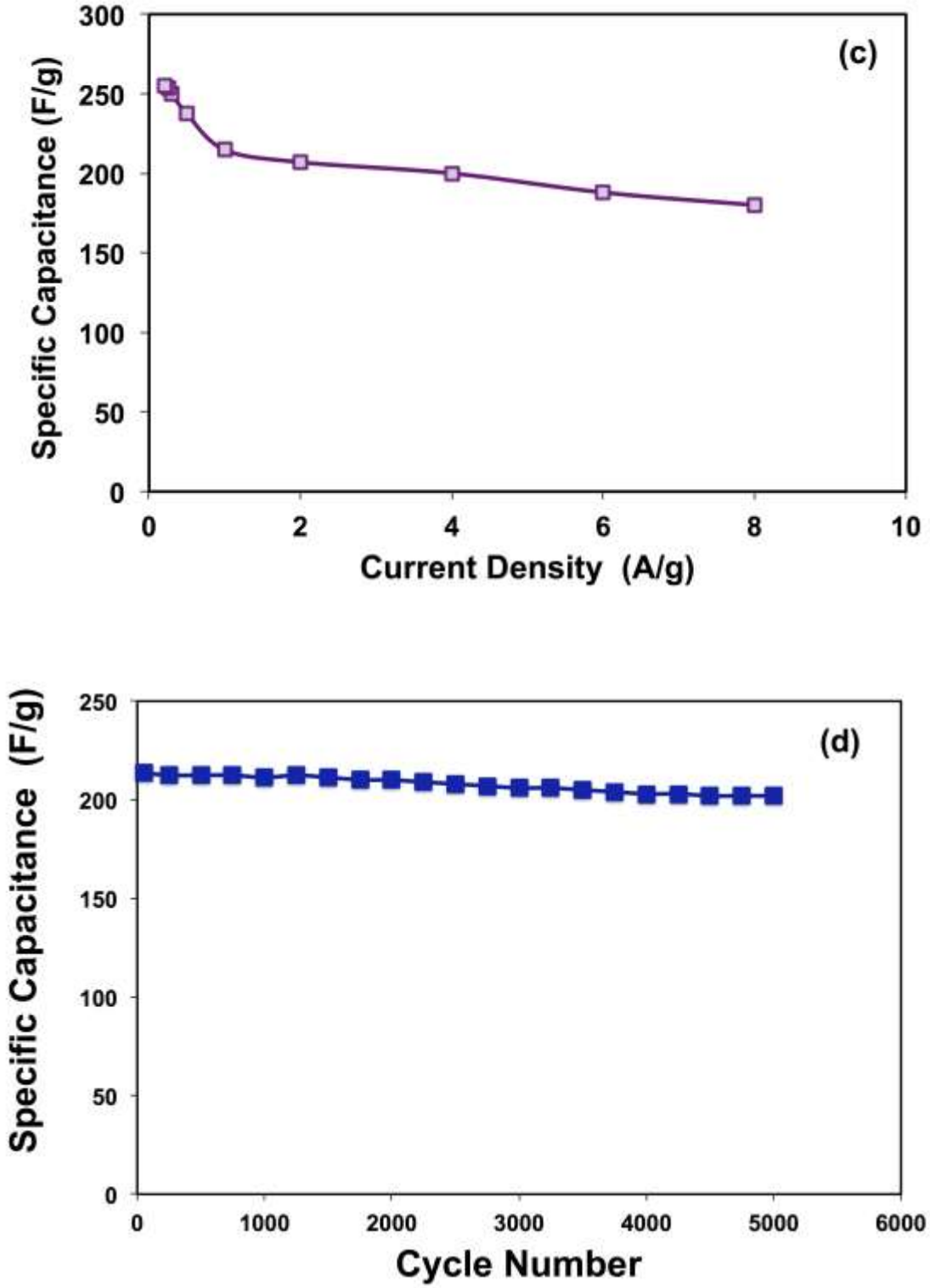

Figure 8: Supercapacitance performance of the EDoX-GO electrode measured in 6 M KOH electrolyte. (a) CV curves for different scan rates from 20 to 150 mV/S showing rectangular shapes revealing of ideal double layer capacitive behaviour, and the absence of redox couple peaks. (b) Galvanostatic charge/discharge under different constant current values, showing fast charge transfer rates and the absence of an observable voltage drop. (c) Specific capacitance as a function of the current densities calculated from the corresponding discharge curve for each current density. (d) Cycling stability of the supercapacitor at 1 A g^{-1} constant current cycling. Retention of 95% was obtained after 5,000 cycles.

Materials and methods

Synthesis of reduced graphene oxide

GO was synthesised from natural graphite by a modified Hummers method as described elsewhere.[42, 43] The electrochemical experiments were conducted in a molten salt reactor consisting of a vertical tubular Inconel® vessel with 70 mm inside diameter and 600 mm height placed inside a Vecstar® ceramic-lined 100 mm vertical tube furnace (Figure S1 in the supporting information). Further details about the electrochemical setup can be obtained elsewhere.[44] The cathode was assembled by manually pressing 200 mg of as-synthesised GO into a copper cup (25 mm outside diameter, 21 mm inside diameter, 7 mm height, and 3 mm thick with many 2 mm holes) (figure S2 in the supporting information). The copper cup was then wrapped in copper mesh, and connected to a stainless steel rod through an M3 thread drilled on the side of the copper cup.

The electrolyte used, KCl–LiCl, was prepared by stirring the eutectic composition for 24 hours then heating under vacuum for 12 hours. The dry salt was packed in an aluminium crucible and heated to 200 °C, then introduced into the reaction vessel. The vessel was then sealed and argon gas was flushed into the reactor for 5 hours to purge the system of atmospheric air. The furnace temperature was then ramped to 150°C by 2°C/min and kept at this temperature for 12 hours before it was ramped again to 370°C at a rate of 5 °C /min. Once the maximum temperature was achieved, two Pt electrodes were lowered and the salt was subjected to a pre-electrolysis process at 1.5 V for 4 hours to remove metallic impurities and any remaining moisture. After finishing the pre-electrolysis, a fresh Pt wire anode and the cathode assembly were lowered into the molten electrolyte. The electrochemical experiments were conducted with constant voltage chronoamperometry using a PSS-210-GW INSTEK programmable power supply equipped with Instek PSU software. After electrolysis, the cathode assembly was lifted out of the molten electrolyte into the water-cooled part of the reactor. This rapidly quenched the graphene sample to room temperature with electrolyte trapped in between the

sheets. The samples were then removed from the reactor, washed with 3 L distilled water and then leached with dilute HCl assisted by vacuum impregnation to remove the attached solidified electrolyte residue. The samples were then dried overnight under vacuum at 60°C.

Characterisation

X-ray photoelectron spectroscopy (XPS) was done using a Kratos Axis Ultra X-ray photoelectron spectrometer equipped with an aluminium/magnesium dual anode and a monochromated aluminium X-ray source. Fourier-transform infrared (FTIR) spectroscopy was performed at room temperature using a Varian 3100 FTIR spectrometer. The samples were ground with KBr and then pressed into disks. Thermogravimetric analysis (TGA) was performed using Jupiter Netzsch STA 449 C instrument heated at 10°C/min from room temperature to 700°C under nitrogen gas flow. X-ray diffraction (XRD) analysis was conducted using a Philips X'PERT APD powder X–ray diffractometer (λ = 1.54 Å, CuKα radiation). Raman spectra were obtained using a Renishaw 1000 spectrometer coupled to a 633 nm He-Ne laser. The laser spot size was ~1−2 μm, and the power was approximately 1 mW when the laser was focused on the sample using an Olympus BH-1 microscope. Scanning electron microscopy (SEM) was performed using a Philips XL30 FEG SEM, operating at an accelerating voltage of 5 kV. The N2 adsorption–desorption isotherms of the samples were measured at 77 K using ASAP 2020. The specific surface area was calculated from the Brunauer– Emmett–Teller (BET) plot of the nitrogen adsorption isotherm and the pore size distribution of the samples was calculated from adsorption branch isotherms by Barrett–Joyner–Halenda (BJH) method.

Electrochemical measurements

The electrochemical measurement was performed on an Iviumstat Electrochemical Interface with 6 M KOH solution as the aqueous electrolyte using a two-electrode configuration. The working electrode was composed of 75wt% of the prepared material, 20wt% of carbon black, and 5wt% of polytetrafluoroethylene (PTFE) binder, which were mixed together in ethanol and coated onto a nickel foam current collector and then dried at 100°C for 12 hours in a vacuum oven. The typical mass loading of the active material was between 4 and 6 mg cm^2.

Conclusion

Crumpled graphene was prepared with an affordable and scalable electrochemical process. By polarising GO at the cathode at potential high enough to generate reducing alkali metal (3.2 V vs. Pt pseudoreference electrode) in molten LiCl–KCl at 370°C, the oxygen content was reduced from ~30 at% to less than 5 at%. A direct electro-deoxygenation method was also tested at lower potential and removed most oxygen functional groups. The electric conductivity of a film made from the electro-deoxygenated GO was 2300 S/m^2. Interestingly, by quenching the cathode to room temperature, the powder obtained was loose and maintained a high level of convolution and wrinkles that prevented agglomeration and re-stacking resulting in a surface area as high as 565 m^2/g. Because of this highly accessible surface area, the obtained graphene derivative showed excellent capacitive performance with specific gravimetric capacitance as high as 255 F/g without doping with other atoms. It also showed long cycle life along with ~95% capacitance retention after 5000 cycles.

References:

1. A. K. Geim, *Science*, 2009, 324, 1530-1534.
2. A. K. Geim and K. S. Novoselov, *Nature Materials*, 2007, 6, 183-191.
3. M. D. Stoller, S. Park, Z. Yanwu, J. An and R. S. Ruoff, *Nano Letters*, 2008, 8, 3498-3502.
4. J. Yan, J. Liu, Z. Fan, T. Wei and L. Zhang, *Carbon*, 2012, 50, 2179-2188.
5. D. Chen, H. Feng and J. Li, *Chemical Reviews*, 2012, 112, 6027-6053.
6. A. Bello, O. O. Fashedemi, J. N. Lekitima, M. Fabiane, D. Dodoo-Arhin, K. I. Ozoemena, Y. Gogotsi, A. T. Charlie Johnson and N. Manyala, *AIP Advances*, 2013, 3, 082118.
7. L. Zhang and G. Shi, *The Journal of Physical Chemistry C*, 2011, 115, 17206-17212.
8. Z. Lei, L. Lu and X. S. Zhao, *Energy & Environmental Science*, 2012, 5, 6391-6399.
9. S. R. C. Vivekchand, C. S. Rout, K. S. Subrahmanyam, A. Govindaraj and C. N. R. Rao, *J. Chem. Sci.*, 2008, 120, 9-13.
10. Y. Zhu, S. Murali, M. D. Stoller, K. J. Ganesh, W. Cai, P. J. Ferreira, A. Pirkle, R. M. Wallace, K. A. Cychosz, M. Thommes, D. Su, E. A. Stach and R. S. Ruoff, *Science*, 2011, 332, 1537-1541.
11. Z. Lin, Y. Liu, Y. Yao, O. J. Hildreth, Z. Li, K. Moon and C.-p. Wong, *The Journal of Physical Chemistry C*, 2011, 115, 7120-7125.

12. I. N. Kholmanov, C. W. Magnuson, A. E. Aliev, H. Li, B. Zhang, J. W. Suk, L. L. Zhang, E. Peng, S. H. Mousavi, A. B. Khanikaev, R. Piner, G. Shvets and R. S. Ruoff, *Nano Letters*, 2012, 12, 5679-5683.
13. H.-F. Ju, W.-L. Song and L.-Z. Fan, *Journal of Materials Chemistry A*, 2014, 2, 10895-10903.
14. Q. Wu, Y. Xu, Z. Yao, A. Liu and G. Shi, *ACS Nano*, 2010, 4, 1963-1970.
15. J. Yan, T. Wei, B. Shao, Z. Fan, W. Qian, M. Zhang and F. Wei, *Carbon*, 2010, 48, 487-493.
16. Y. Si and E. T. Samulski, *Chemistry of Materials*, 2008, 20, 6792-6797.
17. J. Yan, T. Wei, W. Qiao, B. Shao, Q. Zhao, L. Zhang and Z. Fan, *Electrochimica Acta*, 2010, 55, 6973-6978.
18. D. Wang, R. Kou, D. Choi, Z. Yang, Z. Nie, J. Li, L. V. Saraf, D. Hu, J. Zhang, G. L. Graff, J. Liu, M. A. Pope and I. A. Aksay, *ACS Nano*, 2010, 4, 1587-1595.
19. H. Wang, H. S. Casalongue, Y. Liang and H. Dai, *Journal of the American Chemical Society*, 2010, 132, 7472-7477.
20. H. J. Kim, H. Randriamahazaka and I. K. Oh, *Small*, 2014, 10, 5023-5029.
21. A. M. Abdelkader, C. Vallés, A. J. Cooper, I. A. Kinloch and R. A. W. Dryfe, *ACS Nano*, 2014, 8, 11225-11233.
22. C. W. Bale, P. Chartrand, S. A. Degterov, G. Eriksson, K. Hack, R. Ben Mahfoud, J. Melançon, A. D. Pelton and S. Petersen, *Calphad: Computer Coupling of Phase Diagrams and Thermochemistry*, 2002, 26, 189-228.
23. D.-Q. Yang and E. Sacher, *Langmuir*, 2005, 22, 860-862.
24. J. Zhao, S. Pei, W. Ren, L. Gao and H. M. Cheng, *ACS Nano*, 2010, 4, 5245-5252.
25. A. M. Abdelkader, K. T. Kilby, A. Cox and D. J. Fray, *Chemical Reviews*, 2013, 113, 2863-2886.
26. T. B. Joseph, N. Sanil, L. Shakila, K. S. Mohandas and K. Nagarajan, *Electrochimica Acta*, 2014, 139, 394-400.
27. B. H. Park, S. B. Park, S. M. Jeong, C. S. Seo and S. W. Park, *Journal of Radioanalytical and Nuclear Chemistry*, 2006, 270, 575-583.
28. S. Stankovich, R. D. Piner, X. Chen, N. Wu, S. T. Nguyen and R. S. Ruoff, *Journal of Materials Chemistry*, 2006, 16, 155-158.
29. A. G. Hsieh, C. Punckt, S. Korkut and I. A. Aksay, *The Journal of Physical Chemistry B*, 2013, 117, 7950-7958.
30. A. G. Hsieh, S. Korkut, C. Punckt and I. A. Aksay, *Langmuir*, 2013, 29, 14831-14838.
31. A. M. Abdelkader, I. A. Kinloch and R. A. W. Dryfe, *Chemical Communications*, 2014, 50, 8402-8404.
32. V. H. Pham, H. D. Pham, T. T. Dang, S. H. Hur, E. J. Kim, B. S. Kong, S. Kim and J. S. Chung, *Journal of Materials Chemistry*, 2012, 22, 10530-10536.
33. H. L. Poh, F. Šaněk, A. Ambrosi, G. Zhao, Z. Sofer and M. Pumera, *Nanoscale*, 2012, 4, 3515-3522.
34. W. Chen, L. Yan and P. R. Bangal, *Carbon*, 2010, 48, 1146-1152.
35. A. C. Ferrari, *Solid State Communications*, 2007, 143, 47-57.
36. A. C. Ferrari and D. M. Basko, *Nature Nanotechnology*, 2013, 8, 235-246.
37. A. Jorio, E. H. M. Ferreira, M. V. O. Moutinho, F. Stavale, C. A. Achete and R. B. Capaz, *physica status solidi (b)*, 2010, 247, 2980-2982.

38. C. Gómez-Navarro, R. T. Weitz, A. M. Bittner, M. Scolari, A. Mews, M. Burghard and K. Kern, *Nano Letters*, 2007, 7, 3499-3503.
39. S. Park, J. An, J. R. Potts, A. Velamakanni, S. Murali and R. S. Ruoff, *Carbon*, 2011, 49, 3019-3023.
40. K. H. An, W. S. Kim, Y. S. Park, Y. C. Choi, S. M. Lee, D. C. Chung, D. J. Bae, S. C. Lim and Y. H. Lee, *Advanced Materials*, 2001, 13, 497-500.
41. X. Du, P. Guo, H. Song and X. Chen, *Electrochimica Acta*, 2010, 55, 4812-4819.
42. W. S. Hummers Jr and R. E. Offeman, *Journal of the American Chemical Society*, 1958, 80, 1339.
43. S. Park, J. An, R. D. Piner, I. Jung, D. Yang, A. Velamakanni, S. T. Nguyen and R. S. Ruoff, *Chemistry of Materials*, 2008, 20, 6592-6594.
44. A. M. Abdelkader and D. J. Fray, *Electrochimica Acta*, 2010, 55, 2924-2931.